sustainability

MDPI

Article

Predicting Cu(II) Adsorption from Aqueous Solutions onto Nano Zero-Valent Aluminum (nZVAl) by Machine Learning and Artificial Intelligence Techniques

Ahmed H. Sadek [1,2], Omar M. Fahmy [3], Mahmoud Nasr [4,5,*] and Mohamed K. Mostafa [3]

[1] Environmental Engineering Program, Zewail City of Science, Technology and Innovation, 6th October City 12578, Egypt
[2] Sanitary and Environmental Engineering Research Institute, Housing and Building National Research Center (HBRC), Dokki, Giza 11511, Egypt
[3] Faculty of Engineering and Technology, Badr University in Cairo (BUC), Cairo 11829, Egypt
[4] Environmental Engineering Department, Egypt-Japan University of Science and Technology (E-JUST), New Borg El-Arab City 21934, Egypt
[5] Sanitary Engineering Department, Faculty of Engineering, Alexandria University, P.O. Box 21544, Bab Sharqi 21526, Egypt
* Correspondence: mahmoud.nasr@ejust.edu.eg; Tel.: +20-1006390400

Abstract: Predicting the heavy metals adsorption performance from contaminated water is a major environment-associated topic, demanding information on different machine learning and artificial intelligence techniques. In this research, nano zero-valent aluminum (nZVAl) was tested to eliminate Cu(II) ions from aqueous solutions, modeling and predicting the Cu(II) removal efficiency (R%) using the adsorption factors. The prepared nZVAl was characterized for elemental composition and surface morphology and texture. It was depicted that, at an initial Cu(II) level (C_o) 50 mg/L, nZVAl dose 1.0 g/L, pH 5, mixing speed 150 rpm, and 30 °C, the R% was 53.2 ± 2.4% within 10 min. The adsorption data were well defined by the Langmuir isotherm model (R^2: 0.925) and pseudo-second-order (PSO) kinetic model (R^2: 0.9957). The best modeling technique used to predict R% was artificial neural network (ANN), followed by support vector regression (SVR) and linear regression (LR). The high accuracy of ANN, with MSE < 10^{-5}, suggested its applicability to maximize the nZVAl performance for removing Cu(II) from contaminated water at large scale and under different operational conditions.

Keywords: adsorption optimization; aluminum-based nanoparticles; Cu(II); linear regression; neural network; support vector regression

Citation: Sadek, A.H.; Fahmy, O.M.; Nasr, M.; Mostafa, M.K. Predicting Cu(II) Adsorption from Aqueous Solutions onto Nano Zero-Valent Aluminum (nZVAl) by Machine Learning and Artificial Intelligence Techniques. *Sustainability* **2023**, *15*, 2081. https://doi.org/10.3390/su15032081

Academic Editors: Francesco Granata and Mohammad Najafzadeh

Received: 2 December 2022
Revised: 4 January 2023
Accepted: 18 January 2023
Published: 21 January 2023

1. Introduction

Most heavy metals contribute to atmospheric and environmental pollution, and their toxicity can be fatal to humans and various living organisms [1,2]. The ions of these metals are bio-accumulative, and extremely persistent in nature, and thus they pose threats to biological bodies living in aquatic environments [3,4]. There is a growing demand for potable water with low levels of toxicants, which necessitates removing metal ions from contaminated water bodies [5]. Copper (Cu) is one of the environmental pollutants deemed most dangerous to health, since it is not only non-biodegradable but also mutagenic, notorious, and carcinogenic [6,7]. The Cu(II) ion levels in aquatic environments should be below 2.0 mg/L to avoid human health issues, such as reduced lung function, renal and liver failures, chronic bronchitis, cancer, and gastrointestinal distress [4]. The main sources of Cu(II) ion pollution are paper and pulp industries, metallurgical mining, petroleum refining, and steelworks [8]. Evaporation, adsorption, precipitation, membrane separation, electrocoagulation, and ion exchange are the common methods employed to eliminate

heavy metals, including Cu ions, from industrial wastewater sources [9,10]. The adsorption-based wastewater treatment method has encouraged researchers' motivation because of its simplicity of implementation and design, easy recovery of heavy metals, relatively low operation cost, and the feasibility of reusing the spent sorbent [11–13]. Adsorption is also characterized by ease of operation, and generation of low amounts of residue (e.g., sludge) [13,14]. The efficiency of heavy metal (e.g., Cu^{2+}) removal from contaminated water using the adsorption method is highly reliant on the characteristics of the adsorbent material [15–17]. These characteristics include fast and adequate adsorption ability, cost-effectiveness, and regeneration/recyclability/reusability [2].

From accessible sorbent materials, nano zero-valent aluminum (nZVAl) has great potential for use in the treatment of contaminated water due to its high reactivity and strong reductive capacity [18,19]. The nZVAl material has been evidenced to be effective in removing non-biodegradable pollutants by generating hydroxyl radicals and sulfate in the aqueous medium [20]. Many researchers have reported that nZVAl was effective in removing phenol, nitrobenzene, perchlorate, chromium(VI), chloride, nitrate, dye compounds, bisphenol A, and hexabromocyclododecane from contaminated water [20–22]. Nanoscale ZVAl is an active and stable metal with a large surface area, having a wide range of versatility and flexibility for in-situ applications. In addition to advanced oxidation processes (AOPs), nZVAl can be used in single or bimetallic systems. For example, nZVAl-based technologies could quickly remove complex organic pollutants that are hardly biodegradable. nZVAl is also considered a potent reducing agent and could be used as a catalyst in wastewater treatment by oxidation processes. Different pollutants can be eliminated from the aqueous medium using nZVAl in Fe/Al, Pd/Al, and Cu/Al bimetallic systems [20]. The performance of nZVAl in minimizing pollution of the aquatic environments should be adequately predicted to ensure proper wastewater treatment under various operational conditions. These operating conditions are controlled by several factors, e.g., nZVAl dosage, treatment period, and solution pH. The values of these factors should also be optimized to maximize the nZVAl treatment patterns within a shorter time and economically feasible costs [21]. The proposed modeling techniques should be flexible and simple to predict the nZVAl treatment performance toward various and broad ranges of heavy metals when receiving non-linear input attributes [22]. It is an essential step to find the appropriate modeling technique that could mitigate the limitations of some adsorption-related operational conditions, such as nanoparticle aggregation, inadequate colloidal stability, and complexity in solid separation from the final supernatants [19].

Prediction of nZVAl performance for heavy metal removal, with high accuracy and efficiency, is an essential task in wastewater treatment. Machine learning is considered a common technique used for predicting Cu(II) removal from aqueous solutions [23,24]. Many researchers have proposed different techniques for water engineering problems, using support vector regression (SVR), linear regression (LR), and artificial neural network (ANN) [25–28]. As such, SVR is a supervised learning algorithm used for prediction purposes based on a two-layer structure. The first and second layers represent a nonlinear kernel weighting on the input attribute series and a weighted sum of the kernel outputs, respectively [25,29]. The LR methods are appropriately employed to predict the concentrations of multiple water quality parameters, either single output or multiple outputs [30,31]. The artificial neural network (ANN) is a promising mathematical model alternative that has been recently applied to capture the nonlinear correlations in the environmental engineering sector [32–35]. For instance, Fan et al. [36] used ANN for forecasting copper elimination from aqueous media using reduced graphene oxide-supported nanoscale zero-valent iron (nZVI/rGO) magnetic nanocomposites. Granata et al. [37] emphasized that machine learning algorithms could be effectively used in predicting the water quality status of urban wastewater effluents, which would be further considered for sizing and scaling up the treatment facility. In addition, several optimization techniques were established to improve the performance and sustainability of the wastewater treatment processes [38,39].

In this research, nZVAl was tested for the first time to eliminate Cu(II) ions from aqueous media under various experimental conditions (water pH, initial Cu^{2+} concentration (C_o), adsorption period, nZVAl dosage, stirring rate, and temperature). The prepared nZVAl materials were characterized regarding surface morphology and elemental composition to evaluate the Cu(II) uptake pathways. Different isotherm and kinetic adsorption models were used to describe the experimental data. This research also compared between machine learning techniques and artificial intelligence (SVR, LR, and ANN) for estimating Cu(II) removal from water by nZVAl. Because performing experiments for several trials is laborious, difficult, and costly, this modeling protocol would enable future researchers to carry out wastewater-associated experiments in a sustainable manner.

2. Materials and Methods

2.1. Preparation of Cu(II) Solution

For batch experiments, 3.928 g of copper sulfate pentahydrate ($CuSO_4 \cdot 5H_2O$; Loba Chemie, India) was dissolved in 1 L of deionized water to provide a copper stock solution (1000 mg/L). This standard solution was gradually diluted with calculated volumes of deionized water to get the required C_o range (10–50 mg/L). Solutions of 0.1 M HCl and 0.1 M NaOH were applied to adapt the water pH between 1.0 and 7.0. The required reagents were purchased from Honeywell Company, Germany, and Sd Fine Chemicals Ltd., India.

2.2. Synthesis of Adsorbent

Nano-scale zero-valent aluminum (nZVAl) particles were synthesized via the sodium borohydride reduction method ($NaBH_4$, Winlab Co., UK) [21,40]. Briefly, aluminum sulfate ($Al_2(SO_4)_3 \cdot 18H_2O$, Loba Chemie, India) was dissolved in distilled water and the mixture was aggressively agitated at 500 rpm by a magnetic bar. The borohydride solution (25 mL) was added drop by drop to an aqueous medium (25 mL) containing aluminum ions (Al^{3+}) by a burette fixed on the stand. This step was employed to reduce the aluminum ions to zero-valent aluminum nanoparticles. Hydrogen gas was evolved following Equation (1), and the solution pH elevated from 2 to 5 at the reaction's completion. Besides, the reaction temperature rose from 20 °C to 32 °C while the reducing agent was being added to the aluminum ion solution. The synthesis reaction could be described as follows:

$$2Al^{3+} + 6BH_4^- + 18H_2O \rightarrow 2Al^0 + 6H_2BO_3^- + 24H^+ + 12H_2 \quad (1)$$

After reaction completion, the mixture was agitated for an additional 20 min to ensure that the reducing agent and the dissolved aluminum ions were completely reacted, forming the precipitated nZVAl. Following that, vacuum filtration was used to remove the produced nZVAl from the reaction medium. Afterward, the nanoparticles were thoroughly rinsed with distilled water, and then three times with ethyl alcohol, followed by drying the nZVAl in an oven at 110 °C for 6 to 8 h. The synthesized nZVAl surface was covered by a small amount of ethyl alcohol for storage, protecting the nanoparticles from further oxidation. The aforementioned steps are summarized in this flow chart (Figure 1).

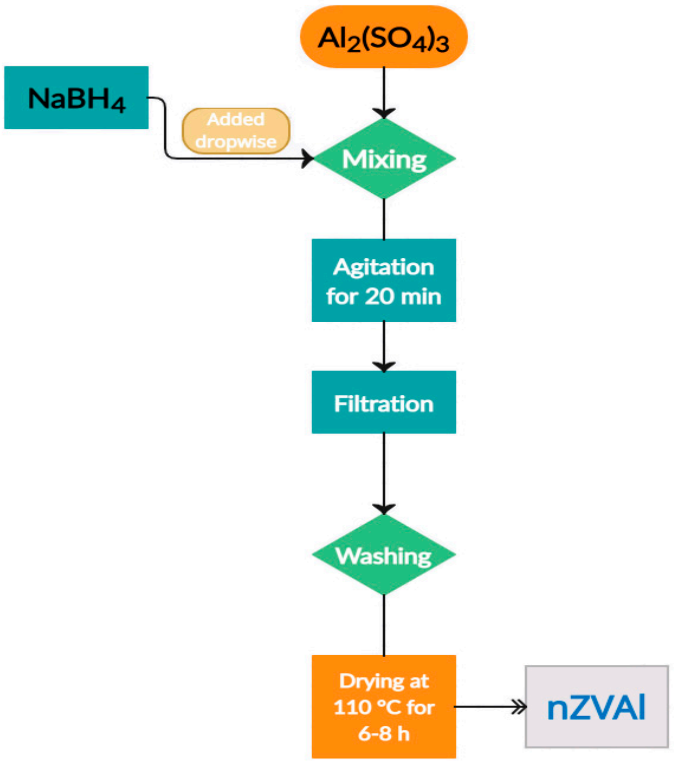

Figure 1. Schematic flow chart representing a synthesis of nZVAl.

2.3. Instrumentation

The particle size and crystal information of nZVAl were examined using X-ray powder diffraction (XRD, Panalytical X'Pert Pro Multipurpose Diffractometer, Netherlands). The equipment was supplied by CuKα radiation with a wavelength of 1.54 Å. The Scherrer equation (Equation (2)) was used to calculate the nZVAl crystallite size [41].

$$D = \frac{K\lambda}{\beta \cos \theta} \quad (2)$$

where D and K represent crystallite size and shape factor, respectively, λ is the X-ray wavelength, β signifies the full width at half-maximum, and θ is the diffraction angle.

A high-resolution transmission electron microscope (HR-TEM, JEM-2100, Japan), operated at 25 kX and 200 kV, was used to explore the nZVAl morphology. A field-emission scanning electron microscope (FE-SEM, Philips, Quanta FEG 250, USA) outfitted with an energy dispersive spectrometer (EDS) was employed at 20 kV to investigate the nZVAl surface structure and elemental composition. The changes in the chemical composition of nZVAl particles, as well as their mineral content and surface atomic distributions, due to adsorption were examined using an X-ray fluorescence (XRF) analyzer (Oxford Instruments, X-MET 7000 series, USA). The supernatant samples, after batch experimentation, were passed through Whatman membrane filters (0.2 µm pore size) and the Cu(II) ion concentrations were measured using a flame atomic absorption spectrophotometer (AAS, Thermo Scientific, ICE 3000 Series AA Spectrometer, USA) at λ = 324.8 nm.

2.4. Experimental Setup

Batch experiments were carried out in 250 mL Erlenmeyer flasks to estimate the effectiveness of nZVAl in removing Cu(II). A one-factor-at-a-time approach was followed to investigate the influences of various experimental factors on Cu(II) removal efficiency (R%), viz., solution pH (1–7), C_o (10–50 mg/L), nZVAl dosage (0.25–1.0 g/L), temperature (30–60 °C), adsorption time (10–60 min), and stirring rate (50–200 rpm). The studied

experimental factors and associated range were assigned based on literature [2,42,43]. All experiments were performed in triplicate.

Equation (3) was employed to compute R(%), whereas Equation (4) was employed to derive the Cu(II) adsorption capacity onto nZVAl.

$$\mathrm{R}(\%) = \frac{\mathrm{C_o} - C_f}{\mathrm{C_o}} \times 100 \tag{3}$$

$$q = \frac{\left(\mathrm{C_o} - C_f\right) \times V}{M} \tag{4}$$

where R(%) is the Cu(II) removal efficiency (%), q is the amount of Cu(II) adsorbed onto nZVAl (mg/g), $\mathrm{C_o}$ and C_f are the initial and final Cu(II) levels in the solutions (mg/L), respectively, M is the nZVAl mass (g), and V is the water volume (L)

2.5. Modelling Techniques

A comparative study between different machine learning techniques and artificial intelligence for estimating R(%) from aqueous media has been carried out. Different regression algorithms, such as SVR, RT, and ANN, have been applied:

2.5.1. Support Vector Regression (SVR)

Support vector regression (SVR) was developed based on the structural risk minimization concept, giving practical applications of statistical learning theory and outstanding generalization performance [44]. SVR aims at finding the hypothesis function, f(x), that separates two different classes in terms of margin maximization. SVR is characterized by its ability to tackle non-linearity relationships and work with non-linear datasets. It uses a linear model to implement non-linear class boundaries through the non-linear mapping of input vectors into a high-dimensional feature space. To tackle this problem, SVR's kernel function and hyperparameters are initially defined. A suitable setting of these parameters will influence the generalization performance of the prediction model. Given an input training dataset, $(X,\ Y) = (x_1,\ y_1),\ (x_2,\ y_2), \cdots,\ (x_N,\ y_N)$, the predicted output response ($\hat{y}$) of $f(x)$ can be expressed by Equation (5) [25,44]:

$$\hat{y} = \langle \omega, \phi(x) \rangle + b = \sum_{i=1}^{N} (\alpha_i k(x_i, x)) + b \tag{5}$$

where $\langle \omega, \phi(x) \rangle$ denotes the dot product of the weight vector (w) and feature vector with a non-linear transformation function $\phi(x)$, α_i coefficients represent the support vectors, $k(x_i,x)$ is a proper kernel function for non-linear feature mapping, and b is a constant term

A polynomial kernel function is used to learn non-linear feature parameters. It compares two column vectors under the objective function framework using a degree-d polynomial formula (Equation (6)) [25]:

$$K(x,\ x') = \left(\gamma x^T x' + c\right)^d \tag{6}$$

where x and x' are two-column vectors representing the feature vectors, γ is a scalar parameter, c is a constant, and d represents the kernel degree. Combining both Equations (5) and (6) to yield $\hat{y}$, as Equation (7):

$$\hat{y} = \langle \omega, \phi(x) \rangle + b = \sum_{i=1}^{N} \left(\alpha_i \left(\gamma x^T x' + c \right)^d \right) + b \tag{7}$$

2.5.2. Linear Regression

Linear regression is a common technique employed to predict an output variable in complicated regression problems [31]. For instance, it could model the relationship between multiple variables to predict the effluent parameters in wastewater treatment processes [31,45,46]. It considers linear predictor functions whose values are derived from the data in the model. The predictor output is commonly a single (dependent) variable. The simple linear regression model is expressed by Equation (8) [30]:

$$Y = \beta_0 + \beta_1 X + \epsilon \tag{8}$$

where Y and X denote the dependent and independent variables, respectively, and β_0 and β_1 are the constant and linear coefficients, respectively, and the symbol ϵ represents the error term.

The model (Equation (9)) for multiple linear regression is:

$$Y = \beta_0 + \beta_1 X_1 + \beta_2 X_2 + \cdots + \beta_m X_m + \epsilon \tag{9}$$

where m denotes the number of regressors.

2.5.3. Artificial Neural Network (ANN)

Artificial intelligence-based techniques are employed for learning, modeling, and predicting a system's performance. The artificial neural network (ANN) is one of these techniques, consisting of input, hidden, and output layers (Figure 2). The neurons in these layers describe the correlation between the input variables and the network's layers [36,47]. Backpropagation is an iterative optimization process, where the loss function and evaluation metric are minimized by adapting the weight and bias between neurons. Mean squared error (MSE) (Equation (10)) was used as a loss metric for evaluating the backpropagation accuracy [28]:

$$\text{MSE} = \frac{1}{N}\sum_{i=1}^{N}(\hat{y} - y_i)^2 \tag{10}$$

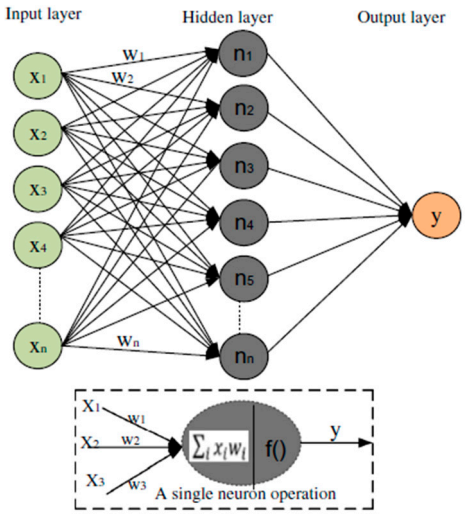

Figure 2. ANN model architecture.

Activation functions were employed to generate a non-linear output from the weighted sum of the ANN's inputs. The input layer was connected to the hidden one using the rectified linear unit (ReLU) activation function, while the linear transfer function was allocated between the hidden and output layer. The number of neurons in the input and hidden layers was chosen to be 6 and 16, respectively, for the best performance of the model. The input data of the ANN model was normalized between −1 and 1 to prevent

numerical overflows because of large or small values of the weights. The normalized equation (Equation (11)) can be defined as follows [36]:

$$y_i = 2\frac{x - x_{\min}}{x_{max} - x_{min}} - 1 \tag{11}$$

where y_i gives the normalized value of x, and $x_{\min}$ and x_{max} stand for the minimum and maximum values of x, respectively.

The weight of a neuron in a certain hidden layer is computed by Equation (12) [36]:

$$W_b = \sum_{a=1}^{k} w_{ab} x_a \tag{12}$$

where k represents the neurons' number in the input layer, w_{ab} is the connection weight between neuron "a" in the input layer and neuron "b" in the hidden layer, and x_a is the neuron "a" value in the input layer.

Similarly, for the output layer, the weight of a neuron in the output layer can be calculated by Equation (13), as follows [36]:

$$W_c = \sum_{b=1}^{z} w_{bc} x_b \tag{13}$$

where z is the number of neurons in the hidden layer, w_{bc} represents the connection weight between neuron "b" in the hidden layer and neuron "c" in the output layer, and x_b signifies the neuron "b" value in the hidden layer.

The weight of neurons in either the hidden layer or output layer was used in the activation function to produce the predicted output (Equation (14)):

$$y = f\,(W + B) \tag{14}$$

where y, f, W, and B are the output, activation function, weight, and bias, respectively.

Although the neurons' number in the hidden layer is directly proportional to the simulation performance of the ANN model, the excessive number of neurons could result in over-fitting. The over-fitting issue tends to lessen the robustness and generalization of the proposed model.

3. Results and Discussion

3.1. Results of the Experimental Characterization

The XRD profile of the nZVAl particles showed different peak intensities (Figure 3a). The three most intense peaks were denoted at 38.4°, 44.6°, 64.9°, and 78.1° for (111), (200), (220), and (311) planes of aluminum, respectively. These peaks could describe the Al^0 face-centered cubic structure of nZVAl. As such, the synthesized aluminum nanoparticles existed in their zero-valent form (Al^0), with a crystalline size of about 34 nm. The minor peaks for 2θ between 20° and 35° could be ascribed to the detection of some trace elements/deposits, such as sodium sulfate (Na_2SO_4), formed during the nanoparticles' preparation. These byproducts could not be completely removed from nZVAl during the washing process. In addition, there is an opportunity that a minor portion of the Al metal was incompletely oxidized throughout the whole synthesis procedure. It is anticipated that the produced nZVAl particles primarily had an amorphous Al_2O_3 outer oxide shell, acting as an inert film to shield Al from unexpected oxidation.

The TEM image of synthesized nZVAl is shown in Figure 3b. The image depicted that the nZVAl particles had rough surfaces, semi-spherical shapes, and diameters ranging from 10 to 100 nm. The individual nanoparticle was approximately 34 nm in diameter, and the majority (almost 80%) of the particles were smaller than 100 nm. In addition, the Al^0 acted as the core of nanoparticles, while the aluminum oxide represented their thin exterior

layer (a shell) [48]. Moreover, some nanoparticles of various sizes and shapes that were haphazardly clustered together developed larger nanoclusters. As such, the greater surface area of the discrete particles may be responsible for these aggregates.

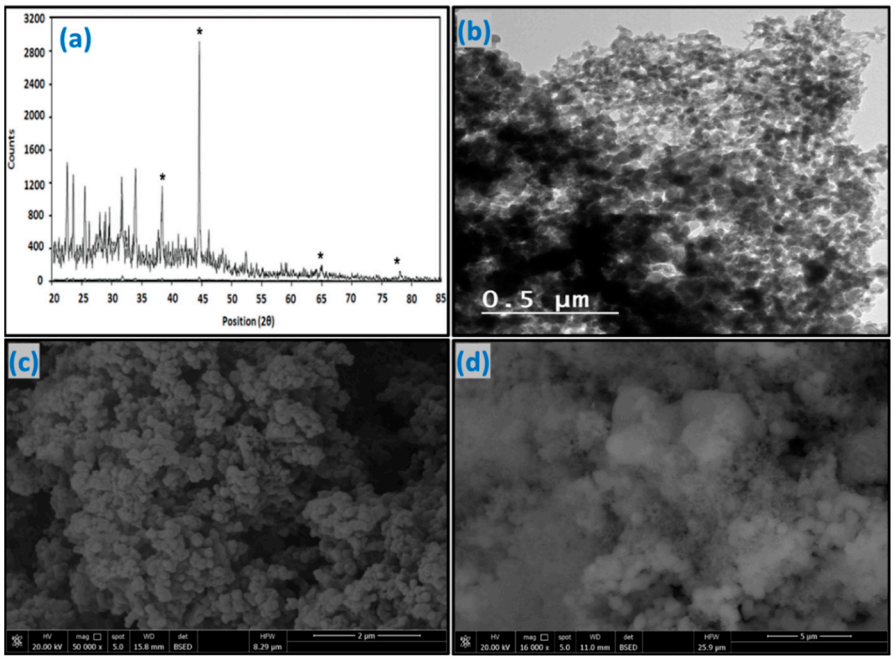

Figure 3. (**a**) XRD, (**b**) TEM, (**c**) SEM image before Cu(II) adsorption, and (**d**) SEM image after Cu(II) adsorption, (*) indicate the position of nZVAl peaks.

Figure 3c displays the SEM image of the unloaded nZVAl nanoparticles. The nanoparticles displayed an irregular surface feature with numerous unequal and noncircular pores. Additionally, certain nanoparticles adhered together (agglomerated), forming chain-like nanoclusters with diameters smaller than 100 nm. Such aggregates have also been noticed for nZVAl preparation [49]. However, this morphological feature was changed when water laden with Cu(II) contacted the nZVAl surface (Figure 3d). For instance, many pores disappeared and the empty zones were filled by Cu(II) ions. This change in surface morphology, with different sizes and shapes of aggregates, could reflect the high adsorption affinity of nZVAl toward Cu(II). In particular, some Cu(II) ions created an attached adsorbate film on the nZVAl outer surface, whereas others migrated through the nanoparticles' interior voids.

EDS spectra were employed to analyze the chemical composition of nZVAl before and after Cu(II) uptake (Figure 4a,b). The use of ethanol (C_2H_6O) during the washing step and/or the nZVAl incomplete oxidation because of material carrying, cleaning, and handling could be responsible for the existence of C and O components. The nZVAl sample consisted of 25.17% aluminum by weight. The presence of a prominent peak at 1.5 keV was mainly attributed to elemental Al, showing that the aluminum element represented the majority of the obtained sample's composition. The formation of peaks for Na, S, Cl, and Cu in the EDS elemental pattern of the loaded adsorbent demonstrated that Cu(II) ions were adsorbed properly onto the nZVAl surface. Additionally, it is possible to recognize that the weight percentage of Al reduced from 25.17% to 18.32% (before and after Cu(II) adsorption). On the contrary, the weight percentage of O increased from 55.99% to 64.16%, respectively. As such, the nZVAl particles were further oxidized and a thicker shell of Al_2O_3 layers was formed.

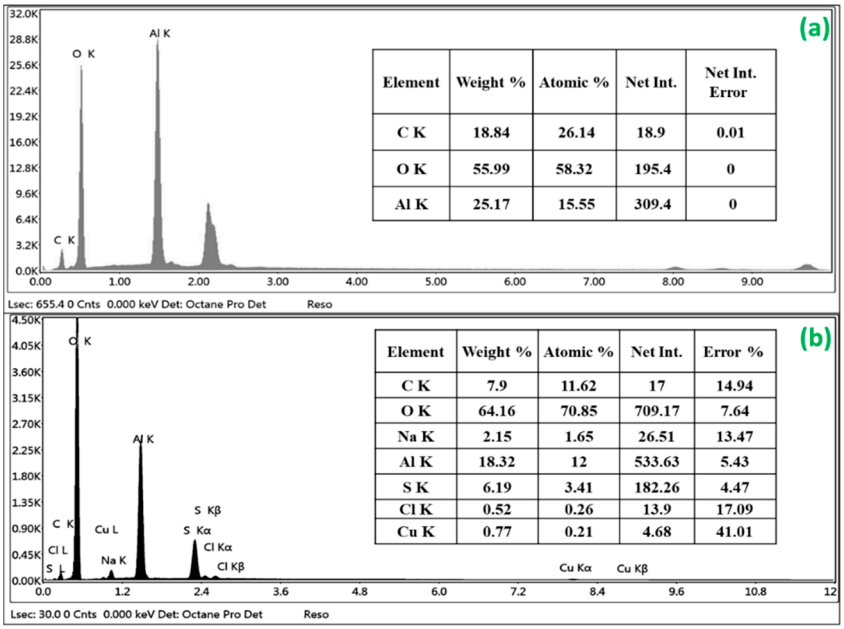

Figure 4. EDS spectrum of nZVAl (**a**) before Cu(II) adsorption, and (**b**) after Cu(II) adsorption.

Table 1 lists the XRF examination results of the mineral oxides forming the nZVAl sample. The sample consisted primarily of the element aluminum, with a percentage of 77.07%, in the form of Al_2O_3, and traces of metal oxides (impurities) that could be disregarded. Additionally, these results supported the prior characterization findings of XRD and EDS analyses and verified that the produced nanoparticles were largely composed of aluminum. Following Cu(II) ion adsorption, the aluminum oxide proportion shifted slightly from 77.07% to 70.12%. However, the nZVAl particles maintained their chemical composition remarkably. This variation in Al content could be ascribed to (i) formation of aluminum oxides during experimental operation that accumulated on the nZVAl surface, and/or (ii) oxidation of the thin layer that immediately surrounded the nZVAl particles' surface followed by subsequent oxidation of the deeper layers. Additionally, the sample comprised copper oxides in the form of tenorite (CuO) at a percentage of 2.94%. These findings confirm the effectiveness of the nZVAl particles to uptake Cu(II).

Table 1. XRF analysis of nZVAl particles before/after Cu(II) adsorption.

	Al_2O_3	SiO_2	P_2O_5	SO_3	Cl	K_2O	CaO	Cr_2O_3	ZnO	FeO or Fe_2O_3	CuO	Loss of Ignition
Before Cu(II) ion adsorption	77.07 ± 3.36	2.46 ± 0.17	0.69 ± 0.03	11.16 ± 0.58	2.89 ± 0.14	0.22 ± 0.01	0.31 ± 0.01	0.04 ± 0.02	0.037 ± 0.002	0	0	5.12 ± 0.27
After Cu(II) ion adsorption	70.12 ± 3.80	2.42 ± 0.15	0.55 ± 0.02	5.07 ± 0.25	4.55 ± 0.17	0	0.28 ± 0.01	0	0.012 ± 0.002	0.06 ± 0.008 or 0.07 ± 0.009	2.94 ± 0.12	14 ± 0.723 or 13.98 ± 0.724

3.2. Effects of Operating Parameters on Cu(II) Removal

The R(%) using nZVAl changed significantly with regard to the variation in the adsorption factors (Figure 5). For example, the R(%) increased from 18.0 ± 0.9% to 40.0 ± 2.5% as pH rose from 1 to 7, respectively (Figure 5a). In an acidic medium with low pH, there is great competition between hydrogen ions (H^+) and Cu^{2+} for adsorption, limiting the adsorbate ions' transfer to the adsorbent binding locations [2,50,51]. An increase in solution pH is normally followed by the dominance of the negatively charged OH^- on the nZVAl surface, facilitating the uptake of Cu(II) ions from the solution [2].

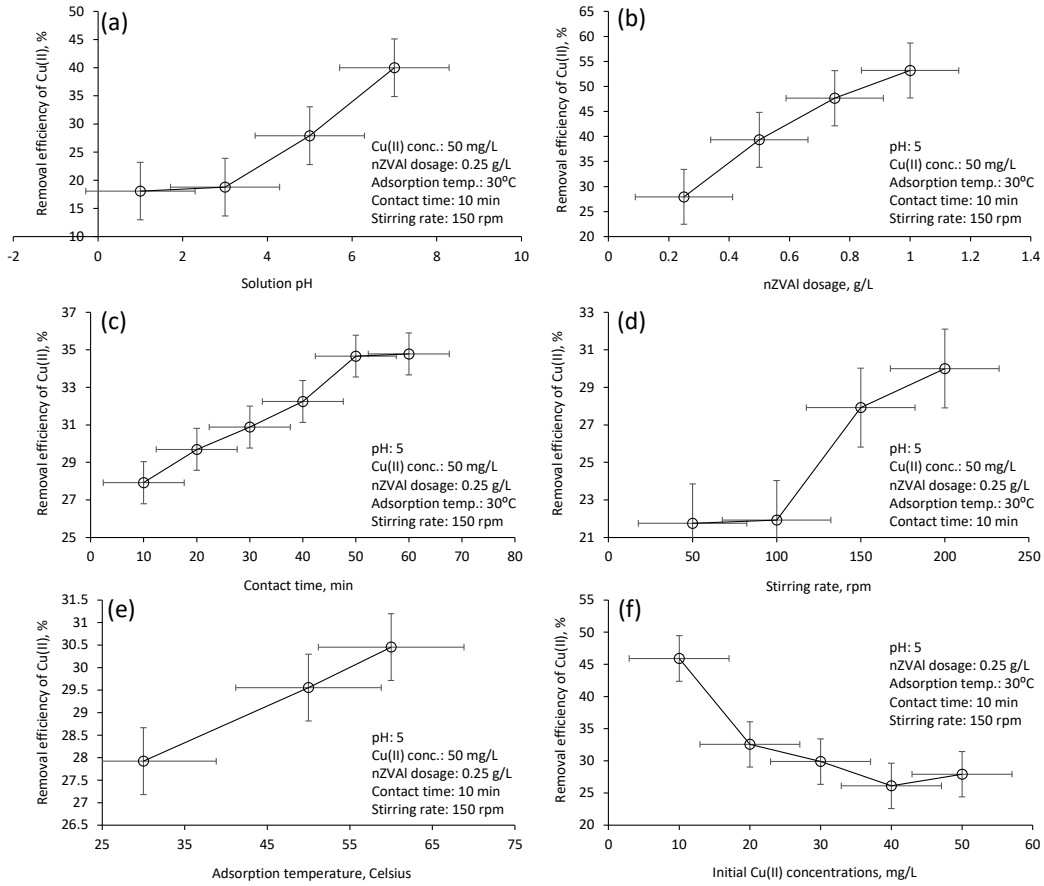

Figure 5. Influences of operational factors on the Cu(II) removal efficiency by nZVAl (**a**) solution pH, (**b**) nZVAl dosage, (**c**) contact time, (**d**) stirring rate, (**e**) adsorption temperature, (**f**) initial Cu(II) concentration.

The R(%) improved from 27.9 ± 1.3% to 53.2 ± 2.4% when the nano-adsorbent dosage increased from 0.25 to 1.0 g/L, respectively (Figure 5b). Elevating the nZVAl dosage created abundant vacant sites that captured larger Cu(II) amounts. A comparable behavior was noticed for Cu(II) ions removal using petroleum coke-derived microporous carbon (adsorbent), depicting an elevation of Cu(II) ions removal from 20 ± 1.1% to 50 ± 2.7% with increasing the dosage from 0.2 to 1.0 g/L, respectively [2].

Contact time is another important factor to be investigated for successfully modeling the adsorption process. The R(%) increased from 27.9 ± 1.3% to 34.7 ± 1.7% when the adsorption time was prolonged from 10 to 60 min, respectively (Figure 5c). The rapid increase in Cu(II) removal during the first 10 min (the initial stage) could be mainly ascribed to the accessibility of more free active sites on the nZVAl surface. The adsorption stage began to reach the equilibrium condition after about 50 min, probably because of nZVAl saturation. Similar behavior was observed for Cu(II) ions removal using chitosan (adsorbent), where the equilibrium state was attained after 50 min of the adsorption period [43].

The R(%) was also improved at faster stirring rates (Figure 5d). A significant improvement in Cu(II) removal from 21.9 ± 1.7% to 27.9 ± 1.8% was observed when the agitation speed was raised from 100 to 150 rpm, respectively. Increasing the stirring rate over 150 rpm also provided a suitable condition for enhancing the diffusion of Cu(II) ions through the nZVAl pores. Similarly, 200 rpm was the optimum stirring speed to improve the solid-liquid phase mass transfer during Cu(II) adsorption onto chitosan [43].

The R(%) also varied according to the shift in the adsorption temperature (Figure 5e). For example, the R(%) was enhanced from 27.9 ± 1.3% to 30.4 ± 1.8% when the adsorption temperature lifted from 30 °C to 60 °C, respectively. This increase in the adsorp-

tion rate could be assigned to the reduction in the activation energy barrier at higher temperatures [52]. Other reasons for the R(%) increase at higher temperatures include (i) development of additional adsorption sites and (ii) increasing the intraparticle diffusion rate of Cu(II) into the adsorbent [51].

The results in Figure 5f showed that the R(%) dropped from 45.9 ± 2.1% to 26.1 ± 1.6% when C_o increased from 10 to 40 mg/L, respectively. At low C_o, the majority of vacant sites are available to capture Cu(II) ions. These findings agree with previous research performing adsorption experimentation by ash to capture Cu(II) from aqueous solutions [53]. Another reason for the R(%) reduction at higher C_o could be the blockage of the available active sites, as well as the increased competition among Cu(II).

3.3. Cu(II) Removal by Various Adsorbents Mentioned in Previous Studies

Table 2 represents a comprehensive comparison between the application of nZVAl and other adsorbents mentioned in the literature for Cu(II) removal from wastewater. At the same experimental conditions, nZVAl exhibited a higher R(%) than groundnut seed cake powder (GNCSP), sesame seed cake powder (SSCP), and coconut cake powder (CCP) [54]. The study [54] focused on preparing biosorbent materials with low costs, which should be further modified to increase their Cu(II) uptake capacities. Most synthetic sorbents exhibited higher R(%) than the natural-based material. Moreover, some adsorbents, such as magnetite nano-adsorbent [55] and TiO_2 nanosorbents [56], exhibited a higher R(%) than nZVAl, even with lower adsorbent dosages. Almost complete Cu(II) removal was observed using nano-TiO_2 sorbent, which could be ascribed to its dual adsorption and photocatalytic activities [56]. The magnetite/carbon nanocomposites exhibited a higher R(%) than nZVAl, but used a higher dosage (0.5 g/L) and longer contact time (240 min) [57]. This variation in R(%) among different adsorbents could be ascribed to the different experimental conditions (e.g., pH, C_o, and adsorbent dosage) and material preparation.

Table 2. Removal efficiencies of Cu(II) using various adsorbent materials reported in the literature.

Adsorbent	Adsorbent Dosage (g/L)	pH	C_o (mg/L)	Time (min)	Temp. (°C)	Stirring Rate (rpm)	Removal Efficiency (%)	Reference
nZVAl	0.25	5	10	10	30	150	45.9	This study
Groundnut seed cake powder (GNCSP)	0.25	5	10	30	40	N/A	43	[54]
Sesame seed cake powder (SSCP)	0.25	5	10	30	40	N/A	40	[54]
Coconut cake powder (CCP)	0.25	5	10	30	40	N/A	41	[54]
Magnetite Nano-Adsorbent from Mill Scale Waste	0.05	5.4	10	30	25	N/A	49	[55]
Titanium oxide (TiO_2) nanosorbents	0.05	6	10	120	25	1000	98	[56]
Bottom ash of expired drugs incineration (BAEDI)	1.0	5	50	15	25	N/A	22	[53]
Magnetite/carbon nanocomposites	0.5	6	10	240	25	N/A	68	[57]

3.4. Cu(II) Removal Mechanism by nZVAl

Generally, Al-water reactions have an induction time, resulting from the hydration of the passive oxide coating on the Al surface. The oxyhydroxide or hydroxide (i.e., H_2O molecules) phases would interact with Al and produce H_2. Consequently, H_2 gas bubbles are generated at the interface between the passive oxide film and inner Al

(Equations (15) and (16)). As the interface reaction proceeds (i.e., the hydration front contacts the surface of the inner Al), the gas pressure in the H_2 bubbles becomes greater than the critical pressure that the dense passive oxide layer can endure. Thus, the H_2 bubbles will collapse to facilitate the transfer of outside water into the Al core [48]. In this scenario, the Al core and Cu(II) ions interact to generate the Cu(II) precipitates (Equations (17) and (18)). H_2 molecules simultaneously depart from the solution and Al surface, creating a macroscopic H_2 gas pressure inside the system. Following the rupture of the passive oxide film, several reactions responsible for Cu(II) reduction possibly happened in light of the aforementioned investigations:

$$Al + 2H_2O \rightarrow AlOOH \downarrow + \frac{3}{2}H_2 \uparrow \quad (15)$$

$$Al + 3H_2O \rightarrow Al(OH)_3 \downarrow + \frac{3}{2}H_2 \uparrow \quad (16)$$

$$Al + Cu^{2+} + 6H_2O \rightarrow Al(OH)_3 \downarrow + Cu(OH)_2 \downarrow + HO^- \quad (17)$$

$$Al^0 + Cu^{2+} \rightarrow Cu \downarrow + Al^{3+} \quad (18)$$

Figure 6 provides a schematic illustration of Cu(II) elimination by nZVAl. It's suggested that Cu(II) removal could follow two different pathways (1) Cu(II) conversion into Cu(II) hydroxides and Cu^0 precipitates, (2) Cu(II) adsorption on the surfaces of thin Al_2O_3 layer or the AlOOH and $Al(OH)_3$ produced by the Al-water reaction. Both the Cu(II) removal and the Al-water reaction compete for the electrons liberated from the metal Al core. According to the current findings, there could be enough electrons from nZVAl available for the elimination of Cu(II).

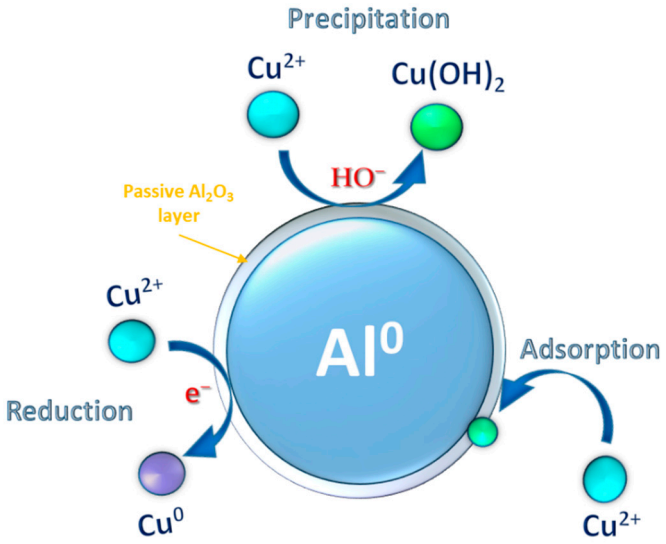

Figure 6. A graphical representation of Cu(II) removal process by nZVAl in aqueous solution.

3.5. Isotherm and Kinetic Investigations

Two isotherm models were applied to demonstrate the adsorption equilibrium between Cu(II) and nZVAl (Figure 7). These models are Langmuir (Equation (19)), and Freundlich (Equation (20)), as previously reported [58]:

$$\frac{C_e}{q_e} = \left(\frac{1}{Q_m}\right)C_e + \frac{1}{K_L \cdot Q_m} \quad (19)$$

$$\log(q_e) = \left(\frac{1}{n}\right)\log(C_e) + \log(K_F) \quad (20)$$

where C_e is the Cu(II) concentration in the aqueous solution at equilibrium (mg/L), Q_m is the maximum adsorption capacity, q_e is the amount of Cu(II) adsorbed per gram of nZVAl at equilibrium (mg/g), K_L is the Langmuir constant (L/mg), K_F is the Freundlich constant (mg/g)·(L/mg)$^{1/n}$, and $1/n$ is the Freundlich constant describing the adsorption intensity/strength.

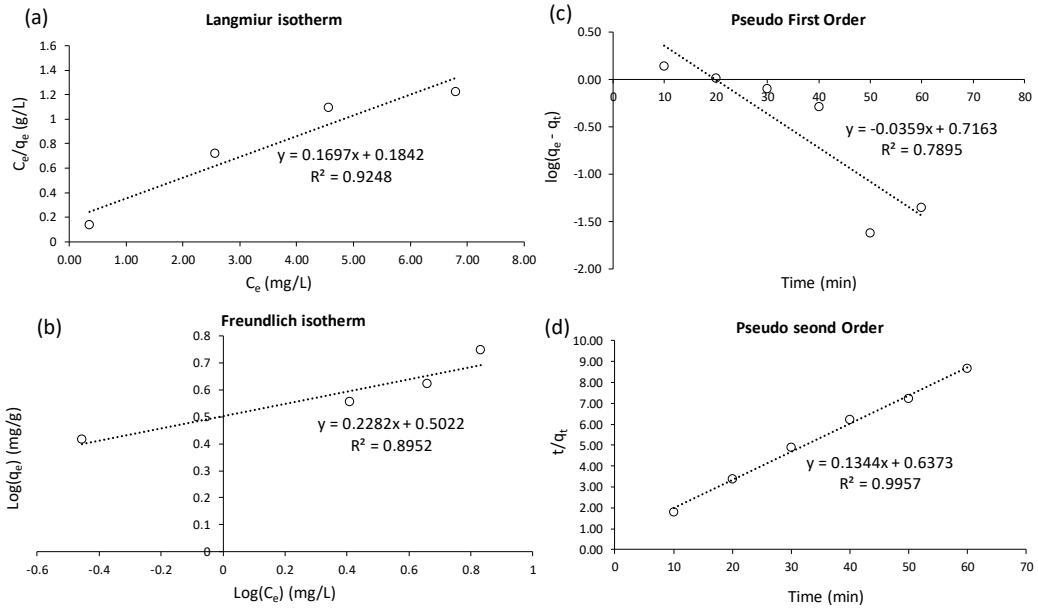

Figure 7. Fitting of adsorption data to (**a**) isotherm Langmuir model, (**b**) isotherm Freundlich model, (**c**) PFO kinetic model, and (**d**) PSO kinetic model.

The Langmuir model attained an adequate fitting accuracy (R^2 = 0.925; Figure 7a) to represent the adsorption isotherm. This fitting suggested that the sorbent surface was homogeneous and Cu(II) uptake by nZVAl could comply with the hypothesis of monolayer adsorption [58,59]. In this context, the model constants (q_m = 5.892 mg/g and K_L = 0.921 L/mg) were suitable to represent the homogeneous adsorption process (Table 3). These constants also indicated that the adsorption of Cu(II) onto nZVAl was preferable under the designed experimental conditions. A low R^2 value for the Freundlich model fit (Figure 7b) suggested that the multilayer adsorption hypothesis could not properly describe Cu(II) removal by nZVAl. The Langmuir model also depicted a better fit to the adsorption results than the Freundlich model for Cu(II) removal using green and red clays [59].

Table 3. Results of isotherm and kinetic studies for Cu(II) removal by nZVAl adsorbent.

Model	Parameter	Fitting Accuracy (R^2)
Langmuir isotherm	q_m = 5.892 mg/g K_L = 0.921 L/mg	0.9248
Freundlich isotherm	$1/n$ = 0.2282 K_F = 3.178 (mg/g)·(L/mg)$^{1/n}$	0.8952
Pseudo-first-order	q_e = 5.2 mg/g k_1 = 0.0826/min	0.7895
Pseudo-second-order	q_e = 7.4 mg/g k_2 = 0.00477 g/mg/min	0.9957

The pseudo-first-order (PFO) (Equation (21)) and pseudo-second-order (PSO) (Equation (22)) kinetic models [60] were applied to quantitatively demonstrate the kinetic adsorption of Cu(II) ions onto nZVAl:

$$\log(q_e - q_t) = \log(q_e) - \frac{k_1}{2.303}t \quad (21)$$

$$\frac{t}{q_t} = \frac{1}{k_2 \times q_e^2} + \frac{1}{q_e} t \quad (22)$$

where q_t and q_e are the amounts of adsorbed Cu(II) at operation time= t and equilibrium, respectively (mg/g), and k_1 (mg/g/min) and (g/mg/min) are rate constants of PFO and PSO, respectively.

The low R^2 value of 0.7895 (Figure 7c) was observed by fitting the experimental data to the PFO kinetic equation, inferring that adsorption didn't occur through diffusion at the solid/liquid interface [61]. The PSO kinetic model achieved a sufficient fitting accuracy (R^2 = 0.9957; see Figure 7d), suggesting that some chemical bonds existed between Cu(II) and the nZVAl's active sites. The derived parameters were k_2 = 0.0283 g/mg/min and $q_{e,calc.}$ = 7.4 mg/g (Table 3). The adsorption of Cu(II) onto magnetite/carbon nanocomposites also followed the PSO kinetic method, with k_2 of 0.00477 g/mg/min and q_e of 9.61 mg/g [57].

3.6. Thermodynamic Study

To determine the thermodynamic properties of Cu(II) adsorption onto nZVAl at various temperatures, Van't Hoff and Gibbs-Helmholtz models were employed at different temperatures of 303, 323, and 333 K. Gibbs free energy (ΔG°), enthalpy (ΔH°), and entropy change in adsorption (ΔS°) are presented by the following Equations (23)–(26) [62]:

$$\Delta G^\circ = \Delta H^\circ - T\Delta S^\circ \quad (23)$$

$$\Delta G^\circ = -RT\ln(K^o) \quad (24)$$

$$\ln K^\circ = \frac{-\Delta H^\circ}{RT} + \frac{\Delta S^\circ}{R} \quad (25)$$

$$K^\circ = \frac{q_e}{C_e} \quad (26)$$

where K° gives the equilibrium constant (mL/g), T represents the absolute temperature (K), and R is the universal gas constant (8.314 J/mol/K). The constants ΔH° (J/mol) and ΔS° (J/mol/K) were determined from a ln(K°) vs. 1/T plot.

Both Figure 8a and Table 4 provide the ΔH° and ΔS° values computed from the slopes and intercepts of ln(K°) against 1/T plot. The K° values changed from 316.32 to 256.70 mL/g when the temperature rose from 303 to 333 K, respectively. Apparently, higher operating temperatures encouraged the interactions between the nZVAl nanoparticles and Cu(II). The Cu(II) removal process was supposed to be endothermic, as depicted by the positive value of ΔH° (+5.77 kJ/mol). In particular, the adsorption process consumes energy because the molecules are diffused rapidly through the solution at relatively higher temperatures. This pattern facilitated the Cu(II) adsorption rate, simultaneously decreasing the adsorption-desorption rate. Additionally, the positive values of ΔS° indicated a propagation in degrees of freedom and randomness on the solid/liquid interface during Cu(II) adsorption onto the nZVAl surface. The value of ΔG° for Cu(II) adsorption onto nZVAl nanoparticles at each temperature is presented in Figure 8b. The negative ΔG° values (−14.50 to −15.35 kJ/mol) indicated that Cu(II) ions removal by nZVAl was feasible and the associated adsorption process could be spontaneous. This change in ΔG° also implied that, within the experimental range, Cu(II) adsorption was thermodynamically preferred at higher temperatures, where the movement of ions absorbed on nZVAl was not restricted.

Table 4. Thermodynamic parameters for Cu(II) adsorption onto nZVAl.

T (K)	K° (mL/g)	ln(K°)	ΔG° (kJ/mol)	ΔH° (kJ/mol)	ΔS° (J/mol/K)	R^2
303	316.32	5.76	−14.50	5.77	66.92	0.997
323	276.72	5.62	−15.10		46.75	
333	256.70	5.55	−15.36		46.13	

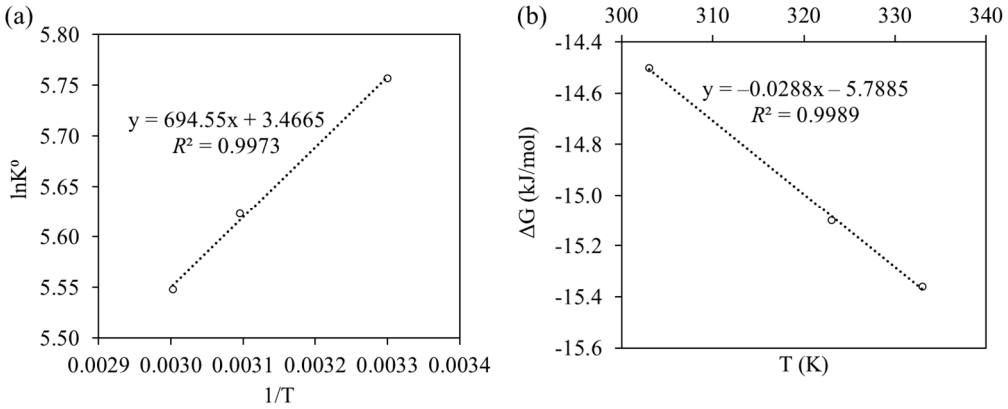

Figure 8. Plots of (**a**) ln(K°) vs. 1/T to give the enthalpy (ΔH°) and entropy (ΔS°), (**b**) Gibbs' free energy change vs. temperature for the adsorption of Cu(II) onto nZVAl.

3.7. Modelling Evaluation Techniques

The data used to build the prediction model for Cu(II) adsorption onto nZVAl consisted of six input factors (pH, time, C_o, nZVAl dose, stirring rate, and temp) and one output parameter, namely R(%). The histogram of the given input and output variables (dataset) is shown in Figure 9. Because the units and ranges of the parameters were different, the dataset was normalized between −1 and 1 using the standard normalization function (see Equation (11)). This step is essential to prevent numerical overflows that might occur from very large or very small weights. The dataset was split into 80% and 20% for the training and testing purposes, respectively.

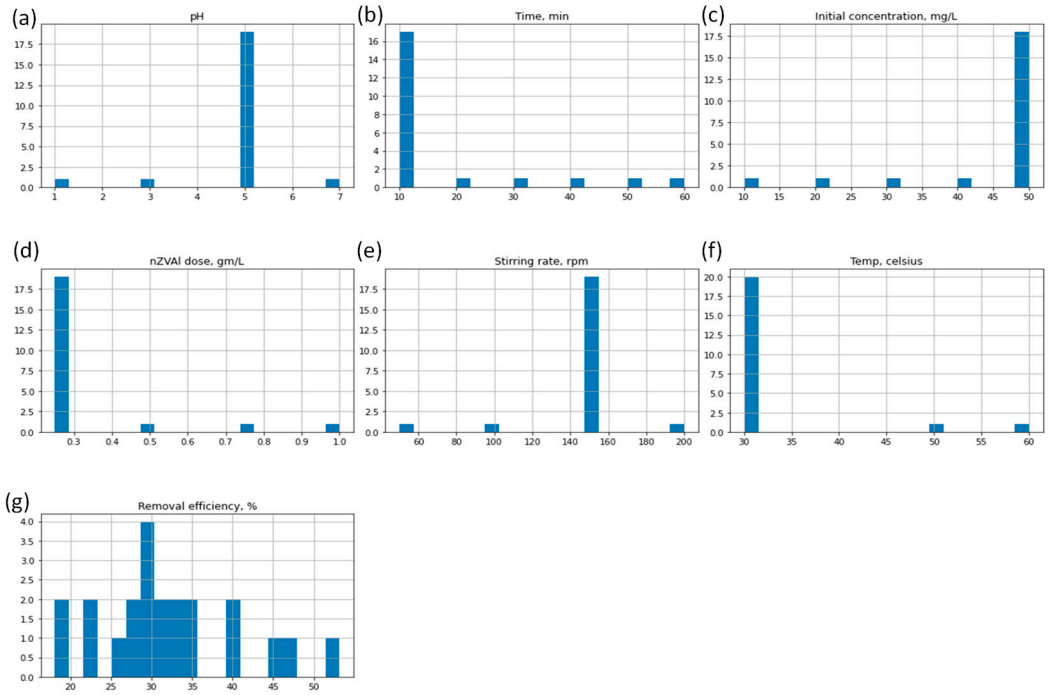

Figure 9. Histogram of input data features (**a**) pH, (**b**) time, (**c**) C_o, (**d**) nZVAl dose, (**e**) stirring rate, (**f**) temperature, and the output variable (**g**) removal efficiency. The y-axis represents frequency (counts) and x-axis denotes the number of bins for each factor.

Initially, the models learn how to predict Cu(II) removal from the training dataset. Then, testing is performed to check the model's performance using new inputs previously unseen during the training process. The ReLU activation function was employed in the hidden layer to provide a non-linear output to the weighted sum of the input-to-hidden

layer. In the final layer, the feature parameters are linearly transferred to the output. The models' hyperparameters are shown in Table 5.

Table 5. Hyperparameters used to predict Cu(II) removal efficiency using six inputs, namely pH, time, C_o, nZVAl dose, stirring rate, and temperature.

ANN Model Parameters	
Hidden layers	3
Activation function	rectified linear unit (ReLU)
Optimizer	Stochastic gradient descent (SGD)
Loss function	Mean Squared Error (MSE)
No. iterations	250
Batch size	32
Weight initializer	Uniform initialization
SVR model parameters	
Kernel type	polynomial (Poly)
Kernel degree	3
γ	'scale'
ϵ	0.1

The MSE was propagated back from the last to the input layer for correcting the values of weights and biases until attaining the maximum number of iterations. The training procedure of the proposed machine learning models was stopped after 2.5 s and tested for their prediction performance with the experimental results. The training trials of the ANN model were equivalent to 250 epochs, yielding the minimum MSE. Table 6 depicts the relationship between the experimental Cu(II) removal efficiencies and the corresponding values derived from the ANN, LR, and SVR models. Table 6 also shows that ANN yielded the best performance with an average MSE error below 10^{-5}, as compared with other models LR (10^{-3}), and SVR (0.01). The ANN model predictions matched the experimental data adequately, whereas other models' predictions didn't maintain similar performance. However, all the proposed models depicted that the highest Cu(II) removal efficiency could be obtained at pH = 5, nZVAl dose of 1.0 g/L, mixing speed = 150 rpm, and 30 °C within 10 min when C_o was 50 mg/L. This highest removal performance complied with the data obtained experimentally, giving R(%) of 53.2%. ANN also succeeded in predicting Cu(II) removal from aqueous media by nanoscale zero-valent iron nanocomposites, offering an adequate accuracy better than the RSM model [36]. The consistency between the ANN predictions and the experimentally measured results may raise the reliability of the proposed ANN model for simulating new input-output correlations.

Table 6. Verification of quadratic regression and ANN models for predicting Cu(II) removal using additional experimental runs.

pH	Time	Initial Concentration (mg/L)	nZVAl Dose (g/L)	Stirring Rate (rpm)	Temp (°C)	Removal Efficiency (%)	ANN R%	LR R%	SVR R%
1	10	50	0.25	150	30	18.1	18.0691	17.6548	18.0466
3	10	50	0.25	150	30	18.8	18.7668	18.3520	18.7438
5	10	50	0.25	150	30	27.9	27.9118	27.4970	27.8888
7	10	50	0.25	150	30	40.0	39.9914	39.5766	39.9684
5	10	50	0.25	150	30	27.9	27.9118	27.4970	27.8888
5	20	50	0.25	150	30	29.7	29.6872	29.2724	29.6642
5	30	50	0.25	150	30	30.9	30.8730	30.4582	30.8500

Table 6. *Cont.*

pH	Time	Initial Concentration (mg/L)	nZVAl Dose (g/L)	Stirring Rate (rpm)	Temp (°C)	Removal Efficiency (%)	ANN R%	LR R%	SVR R%
5	40	50	0.25	150	30	32.2	32.2402	31.8254	32.2172
5	50	50	0.25	150	30	34.7	34.6550	34.2402	34.6320
5	60	50	0.25	150	30	34.8	34.7724	34.3576	34.7494
5	10	10	0.25	150	30	45.9	45.9084	45.4936	45.8854
5	10	20	0.25	150	30	32.6	32.5549	32.1401	32.5319
5	10	30	0.25	150	30	29.9	29.8781	29.4633	29.8550
5	10	40	0.25	150	30	26.1	26.1029	25.6881	26.0799
5	10	50	0.5	150	30	39.3	39.3284	38.9136	39.3054
5	10	50	0.75	150	30	47.7	47.6452	47.2304	47.6222
5	10	50	1.0	150	30	53.2	53.1846	52.7698	53.1616
5	10	50	0.25	50	30	21.8	21.7426	21.3278	21.7196
5	10	50	0.25	100	30	21.9	21.9176	21.5028	21.8946
5	10	50	0.25	200	30	30.0	29.9914	29.5766	29.9684
5	10	50	0.25	150	50	29.6	29.5456	29.1308	29.5226
5	10	50	0.25	150	60	30.5	30.4466	30.0318	30.4236
			MSE				$<10^{-5}$	0.01	10^{-3}

3.8. Future nZVAl-Based Potential Research Perspectives

Traditionally, aluminum-related reagents have often been used as coagulants in the field of water and wastewater treatment. Alum, a salt of aluminum, is a well-known and frequently used coagulant, particularly involved in water purification. Alum is a common coagulant because of its optimum performance at neutral pH and the lack of color-forming complex. However, due to the high reactivity of nZVAl, its use in water and wastewater treatment has recently attracted research attention. Three categories of nZVAl applications can be distinguished in water and wastewater treatment: single system, bimetallic system, and advanced oxidation processes (AOPs). Hence, future studies are required to investigate the scalability of nZVAl to treat industrial effluents, e.g., electroplating wastewater, contaminated with high levels of heavy metals (Figure 10). The presumed full-scale system would comprise four stages: (1) The first stage involves treating real wastewater containing high levels of heavy metals using nZVAl (mixing stage). (2) In the second stage, the treated water is aerated in the presence of H_2O_2, helping in the production of hydroxyl radicals (aeration stage). (3) The third stage consists of a sedimentation tank. (4) The remaining impurities in the clarifier effluent would be removed by sand filters in the last stage. This full-scale system should be investigated to treat large quantities of wastewater with different heavy metal ions and various concentrations. The proposed models in the current study would assist in predicting the performance of the nZVAl scalability dealing with larger quantities of heavy metals-contaminated industrial wastewater.

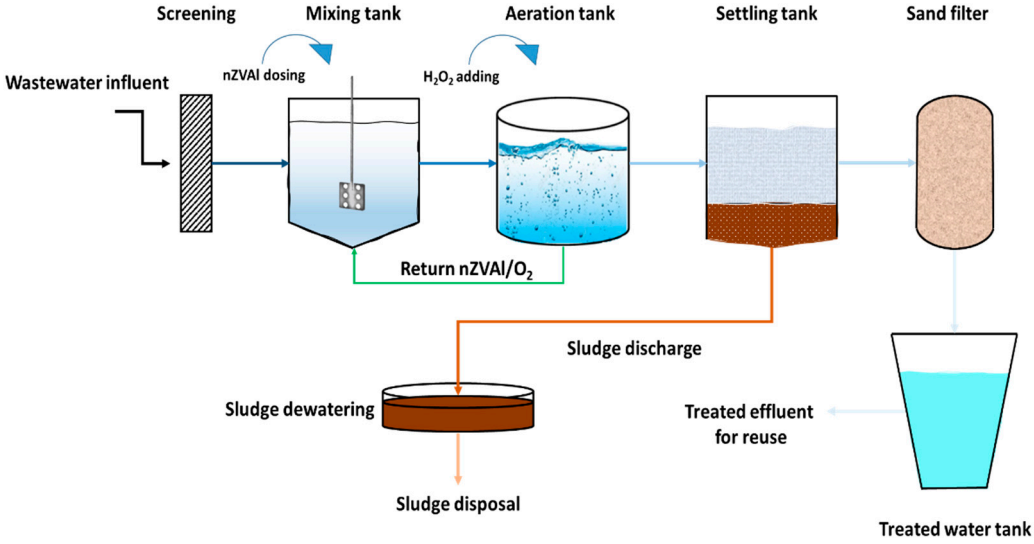

Figure 10. Process flow diagram of the proposed treatment unit of heavy metals-contaminated industrial wastewater using nZVAl.

4. Conclusions

This work focused on using different machine learning techniques and artificial intelligence to predict Cu(II) removal in an adsorption process using nZVAl. The prepared nZVAl was characterized by XRD, TEM, SEM, EDS, and XRF, showing a successful preparation of Al nanomaterials in the zero-valent state. The highest Cu(II) removal efficiency ($53.2 \pm 2.4\%$) was observed at pH = 5, nZVAl dosage = 1.0 g/L, temperature = 30 °C, mixing rate = 150 rpm, and C_o = 50 mg/L within 10 min. The adsorption data were well described by the Langmuir isotherm model (R^2: 0.925, q_m = 5.892 mg/g, and K_L = 0.921 L/mg) and PSO kinetic model (R^2: 0.9957, k_2 = 0.0283 g/mg/min, and $q_{e.}$ = 7.4 mg/g). The three proposed models (ANN, LR, and SVR) were able to accurately predict the Cu(II) removal efficiencies using the same number of input/output variables. However, the ANN technique showed the best prediction performance with MSE < 10^{-5}. These models could be used as a guideline for the industrial sector and stakeholders to overcome the complex issues related to the adsorption process. Although the designed treatment technique proved to be effective in removing Cu(II) from aqueous solutions using nZVAl, two main challenges should be addressed in future research: (i) The efficiency of nZVAl should be evaluated for Cu(II) removal from real wastewater containing other types of contaminants. (ii) The possibility of using nZVAl for consecutive cycles of treatment should be considered.

Author Contributions: Conceptualization, A.H.S., O.M.F. and M.K.M.; methodology, A.H.S., O.M.F., M.N. and M.K.M.; software, A.H.S., O.M.F., M.N. and M.K.M.; validation, A.H.S., O.M.F., M.N. and M.K.M.; formal analysis, A.H.S., O.M.F., M.N. and M.K.M.; investigation, A.H.S., O.M.F., M.N. and M.K.M.; resources, A.H.S., O.M.F. and M.K.M.; data curation, A.H.S., O.M.F. and M.K.M.; writing—original draft preparation, A.H.S., O.M.F. and M.K.M.; writing—review and editing, A.H.S., O.M.F., M.N. and M.K.M.; visualization, A.H.S., O.M.F., M.N. and M.K.M.; supervision, A.H.S., O.M.F., M.N. and M.K.M.; project administration, M.K.M. All authors have read and agreed to the published version of the manuscript.

Funding: This research received no external funding.

Institutional Review Board Statement: Not applicable.

Informed Consent Statement: Not applicable.

Data Availability Statement: Not applicable.

Acknowledgments: The authors would like to thank Badr University in Cairo (BUC), Housing and Building National Research Center (HBRC), and the Zewail City of Science, Technology and Inno-

vation for supporting this research. The third author acknowledges Nasr Academy for Sustainable Environment (NASE).

Conflicts of Interest: The authors declare no conflict of interest.

References

1. Mitra, S.; Chakraborty, A.J.; Tareq, A.M.; Emran, T.B.; Nainu, F.; Khusro, A.; Idris, A.M.; Khandaker, M.U.; Osman, H.; Alhumaydhi, F.A.; et al. Impact of heavy metals on the environment and human health: Novel therapeutic insights to counter the toxicity. *J. King Saud Univ.-Sci.* **2022**, *34*, 101865. [CrossRef]
2. Yuan, X.; Im, S.I.; Choi, S.W.; Lee, K.B. Removal of Cu(II) ions from aqueous solutions using petroleum coke-derived microporous carbon: Investigation of adsorption equilibrium and kinetics. *Adsorption* **2019**, *25*, 1205–1218. [CrossRef]
3. Ma, J.; Qin, G.; Zhang, Y.; Sun, J.; Wang, S.; Jiang, L. Heavy metal removal from aqueous solutions by calcium silicate powder from waste coal fly-ash. *J. Clean. Prod.* **2018**, *182*, 776–782. [CrossRef]
4. Macías-García, A.; Gómez Corzo, M.; Alfaro Domínguez, M.; Alexandre Franco, M.; Martínez Naharro, J. Study of the adsorption and electroadsorption process of Cu (II) ions within thermally and chemically modified activated carbon. *J. Hazard. Mater.* **2017**, *328*, 46–55. [CrossRef] [PubMed]
5. Al-Saydeh, S.A.; El-Naas, M.H.; Zaidi, S.J. Copper removal from industrial wastewater: A comprehensive review. *J. Ind. Eng. Chem.* **2017**, *56*, 35–44. [CrossRef]
6. Parlayıcı; Pehlivan, E. Removal of metals by Fe3O4 loaded activated carbon prepared from plum stone (Prunus nigra): Kinetics and modelling study. *Powder Technol.* **2017**, *317*, 23–30. [CrossRef]
7. Carolin, C.F.; Kumar, P.S.; Saravanan, A.; Joshiba, G.J.; Naushad, M. Efficient techniques for the removal of toxic heavy metals from aquatic environment: A review. *J. Environ. Chem. Eng.* **2017**, *5*, 2782–2799. [CrossRef]
8. Anirudhan, T.S.; Rijith, S. Glutaraldehyde cross-linked epoxyaminated chitosan as an adsorbent for the removal and recovery of copper(II) from aqueous media. *Colloids Surfaces A Physicochem. Eng. Asp.* **2009**, *351*, 52–59. [CrossRef]
9. Pohl, A. Removal of Heavy Metal Ions from Water and Wastewaters by Sulfur-Containing Precipitation Agents. *Water. Air. Soil Pollut.* **2020**, *231*, 1–17. [CrossRef]
10. Madhava Rao, M.; Ramesh, A.; Purna Chandra Rao, G.; Seshaiah, K. Removal of copper and cadmium from the aqueous solutions by activated carbon derived from Ceiba pentandra hulls. *J. Hazard. Mater.* **2006**, *129*, 123–129. [CrossRef]
11. Mostafa, M.K.; Mahmoud, A.S.; Mahmoud, M.S.; Nasr, M. Computational-Based Approaches for Predicting Biochemical Oxygen Demand (BOD) Removal in Adsorption Process. *Adsorpt. Sci. Technol.* **2022**, *2022*, 1–15. [CrossRef]
12. Kamar, M.T.; Elattar, H.; Mahmoud, A.S.; Peters, R.W.; Mostafa, M.K. A critical review of state-of-the-art technologies for electroplating wastewater treatment. *Int. J. Environ. Anal. Chem.* **2022**, 1–34. [CrossRef]
13. Daneshvar, E.; Vazirzadeh, A.; Niazi, A.; Kousha, M.; Naushad, M.; Bhatnagar, A. Desorption of Methylene blue dye from brown macroalga: Effects of operating parameters, isotherm study and kinetic modeling. *J. Clean. Prod.* **2017**, *152*, 443–453. [CrossRef]
14. Hassan, G.K.; Abdel-Karim, A.; Al-Shemy, M.T.; Rojas, P.; Sanz, J.L.; Ismail, S.H.; Mohamed, G.G.; El-gohary, F.A.; Al-sayed, A. Harnessing Cu@Fe3O4 core shell nanostructure for biogas production from sewage sludge: Experimental study and microbial community shift. *Renew. Energy* **2022**, *188*, 1059–1071. [CrossRef]
15. Tee, G.T.; Gok, X.Y.; Yong, W.F. Adsorption of pollutants in wastewater via biosorbents, nanoparticles and magnetic biosorbents: A review. *Environ. Res.* **2022**, *212*, 113248. [CrossRef]
16. Zaimee, M.Z.A.; Sarjadi, M.S.; Rahman, M.L. Heavy Metals Removal from Water by Efficient Adsorbents. *Water* **2021**, *13*, 2659. [CrossRef]
17. Hua, M.; Zhang, S.; Pan, B.; Zhang, W.; Lv, L.; Zhang, Q. Heavy metal removal from water/wastewater by nanosized metal oxides: A review. *J. Hazard. Mater.* **2012**, *211–212*, 317–331. [CrossRef]
18. Deng, D.; Lamssali, M.; Aryal, N.; Ofori-Boadu, A.; Jha, M.K.; Samuel, R.E. Textiles wastewater treatment technology: A review. *Water Environ. Res.* **2020**, *92*, 1805–1810. [CrossRef]
19. Nidheesh, P.V.; Khatri, J.; Anantha Singh, T.S.; Gandhimathi, R.; Ramesh, S.T. Review of zero-valent aluminium based water and wastewater treatment methods. *Chemosphere* **2018**, *200*, 621–631. [CrossRef]
20. Ileri, B.; Dogu, I. Sono–degradation of Reactive Blue 19 in aqueous solution and synthetic textile industry wastewater by nanoscale zero–valent aluminum. *J. Environ. Manag.* **2022**, *303*, 114200. [CrossRef]
21. Sadek, A.H.; Mostafa, M.K. Preparation of nano zero-valent aluminum for one-step removal of methylene blue from aqueous solutions: Cost analysis for scaling-up and artificial intelligence. *Appl. Water Sci.* **2022**, *13*, 1–23. [CrossRef]
22. Mahmoud, A.S.; Farag, R.S.; Elshfai, M.M.; Mohamed, L.A.; Ragheb, S.M. Nano Zero-Valent Aluminum (nZVAl) Preparation, Characterization, and Application for the Removal of Soluble Organic Matter with Artificial Intelligence, Isotherm Study, and Kinetic Analysis. *Air Soil Water Res.* **2019**, *12*, 1–13. [CrossRef]
23. Bhagat, S.K.; Pyrgaki, K.; Salih, S.Q.; Tiyasha, T.; Beyaztas, U.; Shahid, S.; Yaseen, Z.M. Prediction of copper ions adsorption by attapulgite adsorbent using tuned-artificial intelligence model. *Chemosphere* **2021**, *276*, 130162. [CrossRef] [PubMed]
24. Abbasi, E.; Alavi Moghaddam, M.R.; Kowsari, E. A systematic and critical review on development of machine learning based-ensemble models for prediction of adsorption process efficiency. *J. Clean. Prod.* **2022**, *379*, 134588. [CrossRef]
25. Hafsa, N.; Rushd, S.; Al-Yaari, M.; Rahman, M. A Generalized Method for Modeling the Adsorption of Heavy Metals with Machine Learning Algorithms. *Water* **2020**, *12*, 3490. [CrossRef]

26. Mahmoud, A.S.; Farag, R.S.; Elshfai, M.M. Reduction of organic matter from municipal wastewater at low cost using green synthesis nano iron extracted from black tea: Artificial intelligence with regression analysis. *Egypt. J. Pet.* **2020**, *29*, 9–20. [CrossRef]
27. Mahmoud, A.S.; Mohamed, N.Y.; Mostafa, M.K.; Mahmoud, M.S. Effective Chromium Adsorption From Aqueous Solutions and Tannery Wastewater Using Bimetallic Fe/Cu Nanoparticles: Response Surface Methodology and Artificial Neural Network. *Air Soil Water Res.* **2021**, *14*. [CrossRef]
28. Mahmoud, A.S.; Mostafa, M.K.; Peters, R.W. A prototype of textile wastewater treatment using coagulation and adsorption by Fe/Cu nanoparticles: Techno-economic and scaling-up studies. *Nanomater. Nanotechnol.* **2021**, *11*, 1–21. [CrossRef]
29. Yasmin, N.S.A.; Wahab, N.A.; Ismail, F.S.; Musa, M.J.; Halim, M.H.A.; Anuar, A.N. Support Vector Regression Modelling of an Aerobic Granular Sludge in Sequential Batch Reactor. *Membranes* **2021**, *11*, 554. [CrossRef]
30. Mundi, G.; Zytner, R.G.; Warriner, K.; Bonakdari, H.; Gharabaghi, B.; Ayed, L.B.; Golomazou, E.; Karanis, P.; Scheid, P.; Tzoraki, O.; et al. Machine Learning Models for Predicting Water Quality of Treated Fruit and Vegetable Wastewater. *Water* **2021**, *13*, 2485. [CrossRef]
31. Zhang, L.; Ma, X.; Shi, P.; Bi, S.; Wang, C. RegCNN: A Deep Multi-output Regression Method for Wastewater Treatment. In Proceedings of the 2019 IEEE 31st Int. Conf. Tools with Artif Intell, Portland, OR, USA, 4–6 November 2019; Volume 2019, pp. 816–823. [CrossRef]
32. Mahmoud, M.S.; Mahmoud, A.S. Wastewater treatment using nano bimetallic iron/copper, adsorption isotherm, kinetic studies, and artificial intelligence neural networks. *Emergent Mater.* **2021**, *4*, 1455–1463. [CrossRef]
33. Mahmoud, A.S.; Mahmoud, M.S.; Noureldin, A.M.; Peters, R.W.; Mostafa, M.K. (423f) Effective Adsorption of Chromium from Tannery Wastewater Using Green Synthesis Nano-Zero Valent Iron (GT-nZVI) | AIChE Academy. In Proceedings of the 2021 Annual Meeting, 7–19 November 2021. Available online: https://www.aiche.org/academy/conferences/aiche-annual-meeting/2021/proceeding/paper/423f-effective-adsorption-chromium-tannery-wastewater-using-green-synthesis-nano-zero-valent-iron-gt (accessed on 13 October 2022).
34. Mahmoud, M.S.; Mahmoud, A.S.; El-Said, M.A.; Mostafa, M.K. Comparison of aluminum and iron nanoparticles for chromium removal from aqueous solutions and tannery wastewater, empirical modeling and prediction. *Emergent Mater.* **2022**, *5*, 1729–1744. [CrossRef]
35. Farag, R.S.; Elshfai, M.M.; Mahmoud, A.S.; Mostafa, M.K.; Peters, R.W. (592d) Green Synthesis of Nano Iron Carbide: Preparation, Characterization and Application for Removal of Phosphate from Aqueous Solutions. In Proceedings of the 2018 AIChE Annual Meeting, Lawrence Convention Center, Pittsburgh, PA, USA, 28 October–2 November 2018. Available online: https://www.aiche.org/conferences/aiche-annual-meeting/2018/proceeding/paper/592d-green-synthesis-nano-iron-carbide-preparation-characterization-and-application-removal (accessed on 13 October 2022).
36. Fan, M.; Hu, J.; Cao, R.; Xiong, K.; Wei, X. Modeling and prediction of copper removal from aqueous solutions by nZVI/rGO magnetic nanocomposites using ANN-GA and ANN-PSO. *Sci. Rep.* **2017**, *7*, 18040. [CrossRef] [PubMed]
37. Granata, F.; Papirio, S.; Esposito, G.; Gargano, R.; de Marinis, G. Machine Learning Algorithms for the Forecasting of Wastewater Quality Indicators. *Water* **2017**, *9*, 105. [CrossRef]
38. Lotfi, K.; Bonakdari, H.; Ebtehaj, I.; Delatolla, R.; Zinatizadeh, A.A.; Gharabaghi, B. A novel stochastic wastewater quality modeling based on fuzzy techniques. *J. Environ. Health Sci. Eng.* **2020**, *18*, 1099. [CrossRef] [PubMed]
39. Lotfi, K.; Bonakdari, H.; Ebtehaj, I.; Mjalli, F.S.; Zeynoddin, M.; Delatolla, R.; Gharabaghi, B. Predicting wastewater treatment plant quality parameters using a novel hybrid linear-nonlinear methodology. *J. Environ. Manag.* **2019**, *240*, 463–474. [CrossRef]
40. Sadek, A.H.; Mostafa, M. PCT/EG2017/000029 Preparation of Zerovalent Aluminium Nanoparticles at Room Temperature and Uses Thereof. WIPO. 2019. Available online: https://patentscope.wipo.int/search/en/detail.jsf?docId=WO2019057262 (accessed on 14 October 2022).
41. Muniz, F.; Miranda, M.; Santos, C.M.D.; Sasaki, J. The Scherrer equation and the dynamical theory of X-ray diffraction. *Acta Crystallogr. Sect. A Found. Adv.* **2016**, *72*, 385–390. [CrossRef]
42. Ahmad, A.; Rafatullah, M.; Sulaiman, O.; Ibrahim, M.H.; Chii, Y.Y.; Siddique, B.M. Removal of Cu(II) and Pb(II) ions from aqueous solutions by adsorption on sawdust of Meranti wood. *Desalination* **2009**, *247*, 636–646. [CrossRef]
43. Wan Ngah, W.S.; Endud, C.S.; Mayanar, R. Removal of copper(II) ions from aqueous solution onto chitosan and cross-linked chitosan beads. *React. Funct. Polym.* **2002**, *50*, 181–190. [CrossRef]
44. Samanta, B.; Al-Balushi, K.R.; Al-Araimi, S.A. Bearing Fault Detection Using Artificial Neural Networks and Genetic Algorithm. *EURASIP J. Appl. Signal Process.* **2004**, *3*, 366–377. [CrossRef]
45. Yaqub, M.; Eren, B.; Eyupoglu, V. Soft computing techniques in prediction Cr(VI) removal efficiency of polymer inclusion membranes. *Environ. Eng. Res.* **2020**, *25*, 418–425. [CrossRef]
46. Niu, G.; Yi, X.; Chen, C.; Li, X.; Han, D.; Yan, B.; Huang, M.; Ying, G. A novel effluent quality predicting model based on genetic-deep belief network algorithm for cleaner production in a full-scale paper-making wastewater treatment. *J. Clean. Prod.* **2020**, *265*, 121787. [CrossRef]
47. Yaqub, M.; Eren, B.; Eyupoglu, V. Prediction of heavy metals removal by polymer inclusion membranes using machine learning techniques. *Water Environ. J.* **2021**, *35*, 1073–1084. [CrossRef]
48. Yang, Y.; Gai, W.Z.; Zhou, J.G.; Deng, Z.Y. Surface modified zero-valent aluminum for Cr(VI) removal at neutral pH. *Chem. Eng. J.* **2020**, *395*, 125140. [CrossRef]
49. Jiang, Y.; Yang, S.; Liu, J.; Ren, T.; Zhang, Y.; Sun, X. Degradation of hexabromocyclododecane (HBCD) by nanoscale zero-valent aluminum (nZVAl). *Chemosphere* **2020**, *244*, 125536. [CrossRef]

50. Moreno-Piraján, J.C.; Giraldo, L. Adsorption of copper from aqueous solution by activated carbons obtained by pyrolysis of cassava peel. *J. Anal. Appl. Pyrolysis* **2010**, *87*, 188–193. [CrossRef]
51. Bouhamed, F.; Elouear, Z.; Bouzid, J. Adsorptive removal of copper(II) from aqueous solutions on activated carbon prepared from Tunisian date stones: Equilibrium, kinetics and thermodynamics. *J. Taiwan Inst. Chem. Eng.* **2012**, *43*, 741–749. [CrossRef]
52. Alharby, N.F.; Almutairi, R.S.; Mohamed, N.A. Adsorption Behavior of Methylene Blue Dye by Novel CrossLinked O-CM-Chitosan Hydrogel in Aqueous Solution: Kinetics, Isotherm and Thermodynamics. *Polymers* **2021**, *13*, 3659. [CrossRef]
53. Benzaoui, T.; Selatnia, A.; Djabali, D. Adsorption of copper (II) ions from aqueous solution using bottom ash of expired drugs incineration. *Adsorpt. Sci. Technol.* **2018**, *36*, 114–129. [CrossRef]
54. Pavan Kumar, G.V.S.R.; Komal, A.M.; Yerra, B.; Rao, K.S. Removal of Cu(II) using three low-cost adsorbents and prediction of adsorption using artificial neural networks. *Appl. Water Sci.* **2019**, *9*, 44. [CrossRef]
55. Sulaiman, S.; Azis, R.S.; Ismail, I.; Man, H.C.; Yusof, K.F.M.; Abba, M.U.; Katibi, K.K. Adsorptive Removal of Copper (II) Ions from Aqueous Solution Using a Magnetite Nano-Adsorbent from Mill Scale Waste: Synthesis, Characterization, Adsorption and Kinetic Modelling Studies. *Nanoscale Res. Lett.* **2021**, *16*, 1–17. [CrossRef] [PubMed]
56. Ezati, F.; Sepehr, E.; Ahmadi, F. The efficiency of nano-TiO2 and γ-Al2O3 in copper removal from aqueous solution by characterization and adsorption study. *Sci. Rep.* **2021**, *11*, 18831. [CrossRef] [PubMed]
57. Andelescu, A.; Nistor, M.A.; Muntean, S.G.; Rădulescu-Grad, M.E. Adsorption studies on copper, cadmium, and zinc ion removal from aqueous solution using magnetite/carbon nanocomposites. *Sep. Sci. Technol.* **2018**, *53*, 2352–2364. [CrossRef]
58. Duddridge, J.E.; Wainwright, M. Heavy metals in river sediments—calculation of metal adsorption maxima using Langmuir and Freundlich isotherms. *Environ. Pollut. Ser. B Chem. Phys.* **1981**, *2*, 387–397. [CrossRef]
59. Eloussaief, M.; Jarraya, I.; Benzina, M. Adsorption of copper ions on two clays from Tunisia: pH and temperature effects. *Appl. Clay Sci.* **2009**, *46*, 409–413. [CrossRef]
60. Revellame, E.D.; Fortela, D.L.; Sharp, W.; Hernandez, R.; Zappi, M.E. Adsorption kinetic modeling using pseudo-first order and pseudo-second order rate laws: A review. *Clean. Eng. Technol.* **2020**, *1*, 100032. [CrossRef]
61. Simonin, J.-P. On the comparison of pseudo-first order and pseudo-second order rate laws in the modeling of adsorption kinetics. *Chem. Eng. J.* **2016**, *300*, 254–263. [CrossRef]
62. Mathias, P.M. The Gibbs–Helmholtz Equation in Chemical Process Technology. *Ind. Eng. Chem. Res.* **2016**, *55*, 1076–1087. [CrossRef]